RSSI, Vol. 07, N°. 02, December 2018, 18-25

Revue des Sciences et Sciences de l'ingénieur
Journal of sciences and engineering sciences
ISSN 2170-0737/EISSN: 2600-7029
https://www.asjp.cerist.dz/en/PresentationRevue/303

# Electron-monatomic gas scattering cross section for use in ESEM: Application for argon and helium

**Omar. Mansour[a,b*], Zoulikha. Hafsi[a], Abdeddaim. Kadoun[a]**

[a]Laboratoire de Microscopie, Microanalyse de la matière et Spectroscopie Moléculaire, Faculté des Sciences Exactes, Université Djilali Liabès, 22000 Sidi Bel Abbés, Algeria
[b]Université Ziane Achour. Faculté des sciences et de technologies, Route Moudjbara. BP 3117. Djelfa, Algeria

*Article history*
*Submitted date: 2018-05-30*
*Acceptance date: 2018-06-16*

***Abstract***

Optimizing experimental conditions under gaseous environment (low vacuum) is a compulsory step before imaging and performing microanalysis in environmental scanning microscopy, especially at low energy. For this task, simulations Monte Carlo are needed that require the knowledge of cross sections. In this work, the complex optical potential is used to calculate electron-gas scattering cross sections in the low and intermediate energy range for two monatomic gases, argon and helium. Comparisons are made with experimental and theoretical cross sections from the literature. The results show that for helium, the EPT( Extended Previous Theory) model works very well, especially at intermediate energies, which is not the case for the argon gas

***Key-words :*** *Optical Potential; Scattering cross section; ESEM; skirt radius; Monte Carlo*

***Résumé***

L'optimisation des conditions expérimentales sous environnement gazeux (vide poussé) est une étape obligatoire avant l'imagerie et la réalisation de la microanalyse en microscopie à balayage environnemental, notamment à basse énergie. Pour cette tâche, les simulations de Monte Carlo sont nécessaires, et nécessitent la connaissance des sections efficaces. Dans ce travail, le potentiel optique complexe est utilisé pour calculer les sections efficaces de diffusion d'électrons-gaz dans le domaine des énergies faibles et intermédiaires pour deux gaz monoatomiques, l'argon et l'hélium. Des comparaisons sont faites avec des sections efficaces expérimentales et théoriques dans la littérature. Les résultats montrent que pour l'hélium, le modèle EPT (Extended Previous Theory) fonctionne très bien, surtout à des énergies intermédiaires, ce qui n'est pas le cas pour le gaz d'argon.

***Mots-clés :*** *Potentiel optique; section efficace de diffusion; ESEM, rayon de skirt; Monte Carlo*

## 1. Introduction

In order to observe and to characterize materials microstructure with high sensitivity, some developments of new analytical and simulation methods are needed. Working at low and high electron energy regions shows difference in composition and topography behaviour in scanning electron microscopy (SEM) [1, 2]. The acceleration voltage is selected with the aim of minimizing the interaction volume within the sample while still being able to use the K lines for a more accurate quantification. With the fast development of very high brightness guns, it can be possible to perform experiments at very low energy under gaseous environment.

By introducing the gas in an Environmental SEM (ESEM), it is necessary to acquire good understanding of the electron-gas interactions that are responsible for the electron beam scattering so that one can minimize the problems this scattering could cause. The amount of scattering of the primary beam is dependent on a number of parameters among which the gas scattering cross section is of paramount importance since this parameter makes it possible to calculate the details of the electron distribution resulting from the collisions of electrons with gas molecules or atoms. One of the first studies of electron scattering in a low vacuum microscope environment was performed by Moncrieff *et al*. [3] who used differential scattering cross sections (DCS) that were theoretically derived by Lenz in his description of single electron scattering in atomic solids [4]. These Lenz atomic elastic DCSs were based upon Rutherford scattering cross sections that were quantum mechanically modified using theoretical models of Wentzel [5]. The atomic inelastic DCSs used by Moncrieff *et al* were derived from Compton scattering of X-rays for large scattering angles. For small scattering angles they used an analytical expression from Burge & Smith [6]. Gauvin theoretically studied electron scattering to obtain new correction procedures for reducing the effects of skirt formation on quantitative X-ray microanalysis in the ESEM or variable pressure scanning electron microscope (VPSEM) [7]. His theory is based on single electron scattering under the assumption that inelastic collisions are negligible, and therefore most of the beam scattering is caused by elastic collisions. He used screened Rutherford elastic scattering cross sections, which have been shown to be suitable with light elements and therefore for most of the gases used in ESEMs [8]. Monte Carlo simulations showed that elastic scattering can be formulated using simple single scattering theory rather than more complicated plural scattering theory under suitable imaging conditions in an ESEM. The accuracy needed in Monte-Carlo calculations depends on the type of result one is interested in. Appropriate imaging conditions have been defined as when the average number of scattering events per primary electron is less than three [9]. These findings are applicable when one only needs to compute the fraction of unscattered electrons in an electron beam. However if electron beam profiles, skirt distributions and spot sizes are to be derived in ESEM, both elastic and inelastic scattering at a plural level must be considered. Nevertheless, theoretical and experimental studies based on plural scattering were performed [10, 11]. In addition, some authors made experimental measurements of electron scattering in the VPSEM [12, 13].

The DCS may be measured experimentally or calculated theoretically. In previous works [14, 15], we performed calculations of cross sections related to the electron-gas interaction in ESEMs and derived the distribution of the electron spreading inside the sample chamber. The elastic and inelastic DCSs were calculated by means of the equations of Lenz [4] that Jost and Kessler used in determining electron beam distributions in gases [16]. The calculations carried out for various gases in the [5–30 keV] range were in good agreement with experiments. However, when it comes to low or intermediate energy, this approach may not be valid, depending on the chosen gas. In this case, one has to use experimental values of DCSs that unfortunately are not always available. Alternatively, a more efficient theory should be implemented.

This work aims to overcome these difficulties encountered at low and intermediate energy, by using the complex optical potential model for the cross section calculation in monatomic gases, and applying it to argon and helium. The results are compared with experimental reports but also with calculations performed with the theory we previously used and which we have deliberately extended to low energy to assess its validity limit.

## 2. Physical model

When an electron interacts with a target atom, various physical phenomena may occur, owing to the potential developed between the incident and the target electrons and nucleus. When the incoming electron is far from the target, its accompanying electric field affects the target electron cloud distribution, giving rise to induced dipole moment which in turn affects the kinetic motion of the incident electron. This long range potential created by the induced dipole moment is called the polarization potential. At short ranges, as the incident electron approaches the charge cloud of the target, the external electron will encounter two types of potentials: a static potential and an exchange potential. The static potential is generated by the static charge density of the electric cloud, while the exchange potential is due to the exchange effect between the incident and target electrons which become indistinguishable from each other. During the collision processes some particles are absorbed from the incoming electrons due to the inelastic interaction with the target. This can be described approximately by means of an absorptive (negative imaginary) potential called the absorption potential. These potentials are used in the Complex Optical Potential (COP) formalism to obtain the phase shifts and finally the required cross sections. The relativistic Dirac partial-wave calculations for scattering by a local central interaction potential [17], offers the possibility of building the interaction potential by combining different

potentials models. The above-mentioned four potentials are summed together to form the total potential of the scattering system that can be expressed as:

$$V(r) = V_{st}(r) + V_{ex}(r) + V_{cp}(r) + iW_{abs}(r) \quad (1)$$

where $V_{st}$ (r) is the electrostatic potential, Vex (r) is the local exchange potential, $V_{cp}$ (r) is the correlation–polarization potential and $W_{abs}$(r) is the absorption potential represented by the imaginary part of the optical potential, and is calculated from the local-density approximation proposed by Salvat, using the Born–Ochkur approximation and the Lindhard dielectric function to describe the interactions with a free-electron gas, and multiplied by an energy-independent empirical strength factor $A_{abs}$. With an appropriate selection of $A_{abs}$ (The strategy adopted was to allow the strength parameter $A_{abs}$ to take values larger than unity, to account for the effect of the neglected distant interactions), the absorption cross section, obtained from the partial-wave calculation with the aid of the optical theorem, practically equals the inelastic cross section for projectiles with energies from about 100 eV and higher. In the case of elastic scattering by free atoms, this parameter can be determined from experimental elastic DCSs, or if accurate experimental or theoretical values of σabs are available, we can determine the parameter $A_{abs}$ by fitting these data (i.e. by requiring the absorption potential to be consistent with the empirical inelastic cross sections).

It should be noted that the absorption cross section, obtained from this way, practically equals the inelastic cross section for electrons with energies from about 100 eV and higher for $3<A_{abs}<4$.

The scattering of relativistic electrons by the central field V(r) is completely described by the direct and spin-flip scattering amplitudes, given by **[18]:**

$$f(\theta) = \frac{1}{2ik}\sum_l\{(l+1)[exp(2i\delta_{k=-l-1}) - 1] + l[exp(2i\delta_{k=l}) - 1]\}P_l(cos\theta) \quad (2)$$

and

$$g(\theta) = \frac{1}{2ik}\sum_l[exp(2i\delta_{k=l}) - exp(2i\delta_{k=-l-1})]P_l^1(cos\theta) \quad (3)$$

respectively. k is the relativistic wave number of the projectile. $P_l(cos\theta)$ and $P_l^1(cos\theta)$ are Legendre polynomials and associated Legendre function, respectively and δκ is the phase shift. To obtain the values of phase shift δκ, the following coupled differential equations are solved numerically under the appropriate boundary conditions,

$$\frac{dP_{E\kappa}(r)}{d(r)} = -\frac{\kappa}{r}P_{E\kappa}(r) + \frac{E - V_{op} + 2m_ec^2}{c\hbar}Q_{E\kappa}(r) \quad (4)$$

$$\frac{dQ_{E\kappa}(r)}{d(r)} = \frac{E - V_{op}}{c\hbar}P_{E\kappa}(r) + \frac{\kappa}{r}Q_{E\kappa}(r) \quad (5)$$

where κ is the relativistic quantum number and $P_{Eκ}$(r) and $Q_{Eκ}$(r) are the radial functions. E is the kinetic energy of the incident electron and $V_{op}$ is the appropriate complex optical potential which incorporates all the important effects.

The total cross section $\sigma_T$ (for elastic scattering and inelastic absorption) can be obtained from the optical theorem **[19, 20]**,

$$\sigma_T \equiv \sigma_e + \sigma_{Abs} = \frac{4\pi}{K}Imf(0) \quad (6)$$

where

$$\sigma_e = \int \frac{d\sigma}{d\Omega}d\Omega \quad (7)$$

with

$$\frac{d\sigma}{d\Omega} = |f(\theta)|^2 + |g(\theta)|^2 \quad (8)$$

## 3. Monte Carlo Simulation

A Monte Carlo program was used to simulate the electron path in the specimen chamber and to calculate the electron beam skirt at various energies, with pressure of 133Pa. The working distance was taken as 2 mm. Up to $10^5$ electron trajectories were computed at each energy. We investigated the beam profile for argon and helium as a function of the gas pressure and energy. The results from OP model are presented together with EPT one (extended previous theory **[4]**).

The earlier Monte Carlo scheme described **[15]** can be utilized for energies higher than 5 keV. For low energy, it is necessary that the cross-sections utilized to describe the elastic and inelastic scattering are calculated with the partial-wave expansion method. The effect of inelastic absorption on DCSs for elastic scattering has been generally ignored in Monte Carlo studies of electron transport. In the case of electron scattering by free atoms, inelastic absorption causes a substantial reduction of the DCS at intermediate and large angles.

The following analytical expression can be utilized, concerning the use of the relativistic partial-wave expansion method, to expedite the calculations and to approximate the differential elastic scattering cross-section.

$$\frac{d\sigma}{d\Omega} = \Phi(Z,E)\frac{1}{(1-cos\theta+\Upsilon)^2} \quad (9)$$

Note that, with $\Phi(Z,E) = Z^2e^2/4E^2$ and $\Upsilon(Z,E) = 0$, this equation becomes identical to the classical Rutherford formula, while with $\Phi(Z,E) = Z^2e^2/4E^2$ and $\Upsilon(Z,E) = \alpha(Z,E) = (me^4\pi^2/h^2)(Z^{2/3}/E)$, it becomes the screened Rutherford formula. So, as (9) is identical to the equation we used in the previously described Monte Carlo scheme **[15]**, we can use the same formal structure as in that procedure. However, it is necessary that $\Phi(Z,E)$ and $\Upsilon(Z,E)$ are computed in order to obtain, the same values of the total cross-section $\sigma_{el}$ and of the momentum cross-section $\sigma_m$ as calculated by utilizing the quantum-relativistic partial-wave expansion method. Note that these quantities are defined, respectively, by the following:

$$\sigma_{el} = \int \frac{d\sigma}{d\Omega}d\Omega \quad (10)$$

$$\sigma_m = \int(1 - cos\theta)\frac{d\sigma}{d\Omega}d\Omega \ . \quad (11)$$

Therefore, (2) allows one to sample the polar scattering angle with a closed formula:

$$cos\theta = 1 - \frac{2\Upsilon R}{2+\Upsilon-2R} \quad (12)$$

Let us now show how to calculate $\Phi(Z,E)$ and $\Upsilon(Z,E)$ by use of our knowledge of the total elastic scattering cross-section $\sigma_{el}$ and of the momentum elastic scattering cross-section $\sigma_m$ mentioned above. Note that from (9) it follows that

$$\sigma_{el} = \Phi(Z,E)\frac{4\pi}{\Upsilon(2+\Upsilon)} \quad (13)$$

so that the differential elastic scattering cross-section can be rewritten as

$$\frac{d\sigma}{d\Omega} = \frac{\sigma_{el}}{4\pi}\frac{\Upsilon(\Upsilon+2)}{(1-cos\theta+\Upsilon)^2} \quad (14)$$

Using (10) and (14), we obtain, concerning the momentum cross-section,

$$\sigma_m = \sigma_{el}\left[\frac{\Upsilon(\Upsilon+2)}{2}\ln\left(\frac{\Upsilon+2}{\Upsilon}\right) - \Upsilon\right] \quad (15)$$

Let us calculate now the ratio between the momentum elastic scattering cross-section and the total elastic scattering cross-section:

$$\frac{\sigma_m}{\sigma_{el}} = \Upsilon\left[\frac{\Upsilon+2}{2}\ln\left(\frac{\Upsilon+2}{2}\right) - 1\right] \quad (9)$$

The values of $\sigma_m$ and of $\sigma_{el}$ have been numerically calculated, so that it is possible to find the ratio as a function of Z and E. The values of $\Upsilon$ as a function of Z and of the electron energy E can be subsequently computed, by use of our knowledge a bisection algorithm. Once the values of $\Upsilon$ (Z, E) have been stored in a file, it is possible to calculate the value of $\Upsilon$ corresponding to the particle energy at every step of the electron trajectory during the simulation. The sampling of the scattering angle $\vartheta$ can be easily performed by inserting the value of $\Upsilon$ into (12) and selecting a random number uniformly distributed in the range (0, 1) for R.

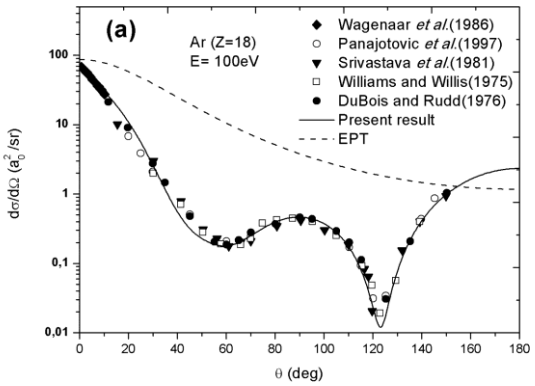
For inelastic scattering event, the Mean Free Path is calculated based on the absorption cross section discussed above. Meanwhile, the inelastic scattering angle, θ is derived from:

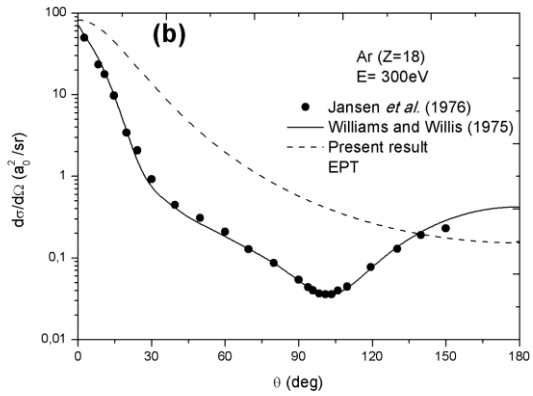
$$\theta = \Delta E/E \quad (10)$$

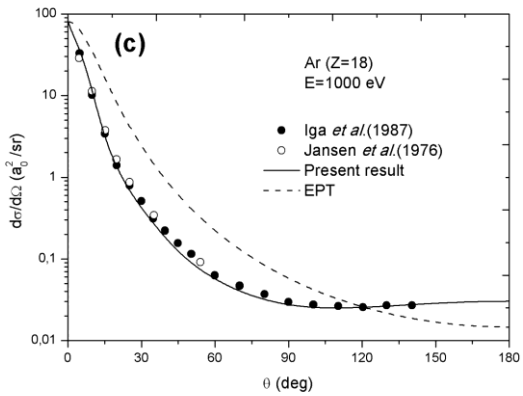
As the electron travel through the gas its energy loses and since the scattering event is energy dependent, the instantaneous energy at any time need to be calculated. The energy loss, for the inelastic and elastic scattering events is taken from [15].

## 4. Results and Discussion

We have computed the total cross section $\sigma_T$ by means of equation (6) and the elastic cross section using equations (7) and (8). By subtracting $\sigma_e$ from $\sigma_T$ we obtain $\sigma_{Abs}$. We have compared our cross section calculation results for argon gas with the experimental measurements of Williams and Willis [21], Srivastava *et al* [22], Dubois and Rud [23], Jansen *et al* [24], Panajotovic *et al*.[25], Wagenaar et al [26] and Iga *et al* [27]. The elastic DCSs calculated with the complex optical potential (Fig.1.a,b,c,d) are clearly in good agreement with the measurements.



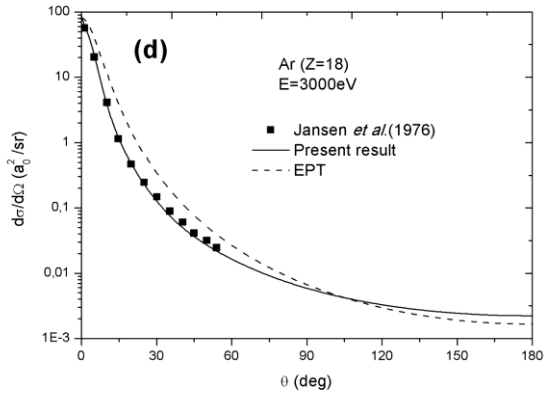



Fig.1. Differential elastic-scattering cross sections of Argon, dσ/dΩ for various incident electron beam energy ranging from 100 eV (a) to 3000 eV (d) ($a_0$ is the Bohr radius)

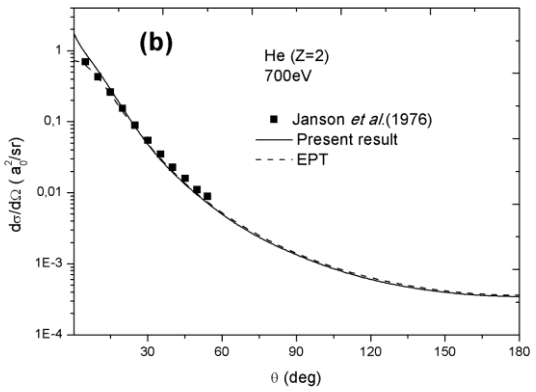
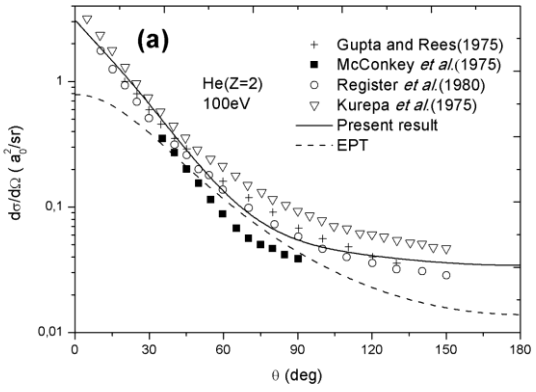



Fig.2. Differential elastic-scattering cross sections of Helium, dσ/dΩ for an incident electron beam energy of 100 eV (a) and 700 eV (b) (a0 is the Bohr radius)

A good agreement between theory and experiment is observed in the general behavior, i.e., both in the shape and absolute nature of the angular distributions of the DCSs.

On the other hand, we have compared the present results with that obtained using our previous approach extended to low energy. This extended previous theory will be labeled EPT hereafter [4]. It is noticeable that the values obtained by EPT are higher than with COP model and that the lower the energy, the higher the difference between the two results. So the differential cross section resulting from the EPT is likely to overestimate the number of electrons scattered in the intermediate angle region. Therefore, the optical potential theory, when involved in the calculation of beam profiles in heavy gases like argon, undoubtedly should strongly contribute to the improvement of the results accuracy, especially at very low energy.




For helium gas, we have also compared our results with the experimental measurements of Gupta and Rees [28], Mc Conkey et al [29], Register et al. [30], Kurepa et al [31], and Jansen et al. [24]. The elastic DCSs calculated with the complex optical potential (Fig.2.a, b) are also clearly in good agreement with the measurements. Here, the EPT curve is almost undistinguishable from the present result even at quite low energy (700 eV), with however a slight difference at very small angles (Fig. 2b). It is only at very low energy (100 eV) that a clear difference appears between the two theories, the present COP results being in better agreement with experiments (Fig. 2a).

Our elastic, absorption, and total cross sections are shown in table 1 for Argon. For comparison aims with experimental values, our calculations have been extended to 10 keV. Also shown in this table are the experimental data of Garcia et al. [32], Wagenaar [33], Kauppila et al. [34], Zecca [35], Nishimura and Yano [36], Wight et al.[13], DuBois et al [23], De Heer et al.[37], Jansen et al.[24] and Iga et al.[27] Overall, our results for total and elastic cross section well agree with the measurements. It is clear that the present results on the σ parameter compare reasonably well with all the displayed experimental points at higher as well as at lower ends of the present energy regime.

Table 1. Argon cross sections ($10^{-20}$ m$^2$)

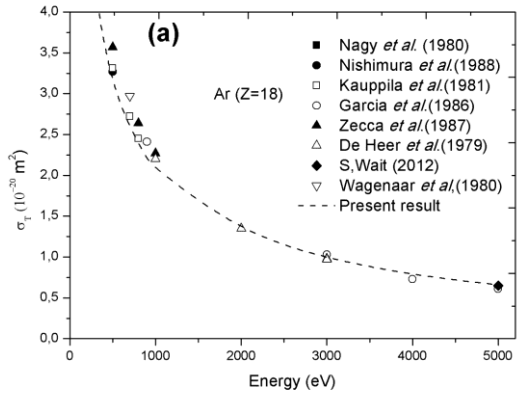
| Energy (eV) | Elastic ($\sigma_e$) | | | Inelastic ($\sigma_{Abs}$) | Total ($\sigma_T$) | | | |
|---|---|---|---|---|---|---|---|---|
| 500 | **1.88** | 2.02 [23] | 1.71 [27] | **1.27** | **3.15** | 3.27 [36] | 3.31 [34] | 3.57 [35] |
| 600 | **1.70** | | | **1.14** | **2.84** | | | |
| 700 | **1.56** | | | **1.02** | **2.60** | 2.97 [33] | 2.72 [34] | |
| 800 | **1.44** | 1.35 [23] | 1.31 [27] | **0.95** | **2.39** | | 2.54 [34] | 2.64 [35] |
| 900 | **1.35** | | | **0.85** | **2.20** | | | |
| 1000 | **1.27** | 1.27 [37] | 1.35 [27] | **0.81** | **2.08** | 2.41 [32] | 2.20 [37] | 2.27 [35] |
| 2000 | **0.82** | 0.80 [35] | | **0.475** | **1.295** | | 1.35 [37] | |
| 3000 | **0.6268** | 0.57 [24] | | **0.358** | **0.9847** | 1.03 [32] | 0.97 [37] | 0.98 [35] |
| 4000 | **0.5124** | | | **0.275** | **0.787** | 0.73 [32] | | |
| 5000 | **0.4353** | | | **0.2237** | **0.66** | 0.61 [32] | 0.65 [13] | |
| 10000 | **0.25** | | | **0.18** | **0.37** | | 0.36 [13] | |

**Table 2**. Helium cross sections ($10^{-20}$ $m^2$)

| Energy (eV) | Elastic ($\sigma_e$) | Inelastic ($\sigma_{Abs}$) | Total ($\sigma_T$) |
|---|---|---|---|
| 500 | **9.92** 9.68 [38] 8.4 [30] 8.6 [39] | **25.18** | **35.10** 37.4 [40-41] 36 [39] |
| 600 | **8.33** 7.0 [39] | **24.10** | **32.43** 32 [39] |
| 700 | **6.93** 6.64 [38] 6.5 [30] 6.0 [39] | **22.34** | **29.27** 29 [39] |
| 800 | **5.99** 5.2 [39] | **20.02** | **26.01** 26 [39] |
| 900 | **5.28** 4.6 [39] | **18.13** | **23.41** 23 [39] |
| 1000 | **4.71** 4.34 [38] 4.1 [30] | **15.78** | **20.49** 21.0 [40-41] 21 [39] |
| 2000 | **2.26** 2.17 [39] | **8.93** | **11.19** 11.1 [40-41] |
| 5000 | **0.88** | **4.32** | **5.20** |
| 10000 | **0.44** | **2.24** | **2.68** 2.4 [42] |

As for helium gas, table 2 shows our results along with the experimental ones of Boesten et al. [38], Register et al. [30], Hayashi **[39]**, Dalba et al. **[40, 41]**, and He and Joy **[42]**.
A very good agreement is observed between the measurements and our COP results for total and elastic cross section.

In figure 3a and b, we have drawn the total cross section according to the energy for argon and helium gas respectively in the 0.1 to 5 keV range. As previously seen from tables 2 and 3, one can observe the good agreement between our calculations and experimental data.



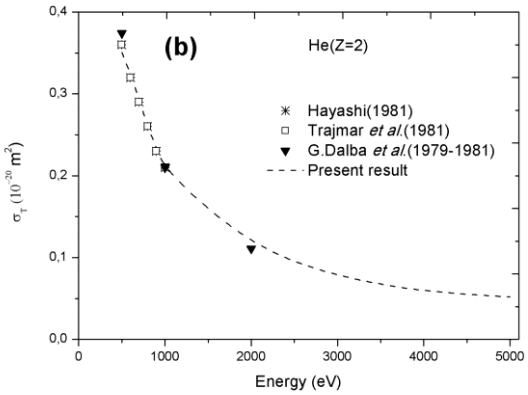




Fig.3. (a) Total cross sections of Argon vs. energy of electron beam (b) Total cross sections of Helium vs. energy of electron beam

By using the two diffusion models mentioned above, we have performed Monte Carlo simulations of the track of electrons incident Argon and helium gases. Our calculations deal with the variation of the skirt radius and unscattered electrons fraction. The skirt radius labelled $r_{0.9}$ was calculated as the radius of the circle on the sample surface containing 90% of the diffused electrons.

In order to continue to compare the influence of different scattering models on the scattering parameters of ESEM as skirt radius and unscattered electrons fraction, we have plotted the skirt radius $r_{0.5}$ vs. the energy.

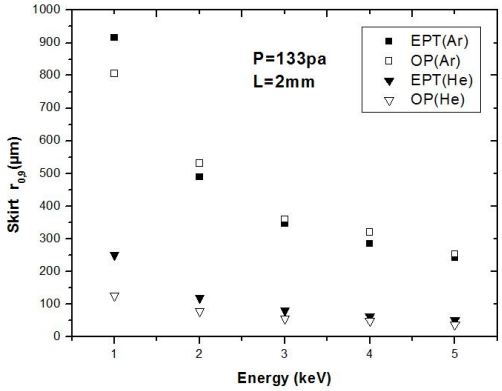



**Fig.4**.Skirt radius vs Energy

Fig.4 shows for the two gases, the skirt radius outcome from EPT and OP model diverge as energy decrease and approaching each other when energy increases. This evolution corroborates the previous profile results obtained for argon and helium elastic cross sections from the two models at high and low energy.

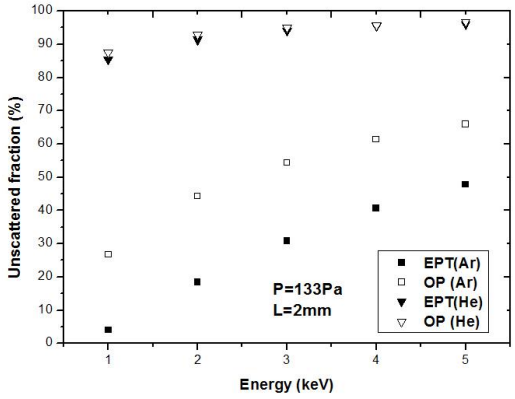



Fig.5.Unscattered electrons fraction vs Energy

From Fig.5, one can see that the unscattered fraction obtained with the OP model is smaller than that obtained with the EPT one, in the case of argon. However, for helium both models give the same result. This fact is due to the similar shape of the two models of the helium scattering cross sections used in the computation.

## Conclusion

We have calculated the elastic electron scattering by Ar and He atoms at low and intermediate energies by employing a complex optical potential approach. The agreement between theory and experiment was observed in the general behavior, i.e., both in the shape and absolute nature of the angular distributions of the differential cross sections and energy dependence. This good agreement between the experimental and our calculated DCSs is fairly encouraging and this model, adapted for molecular gases, will be proposed soon. The calculated scattering cross sections inserted into Monte Carlo simulation program to predict the spatial distribution of the electron beam scattering under given beam energy and gas pressure reveals a large difference in the estimation of the skirt radius at low energy, and the unscattered fraction of the argon with respect to the helium. This difference is due to the invalidity of the EPT model for argon gas, compared to the optical potential one.

## References


[1] Masayasu Nagoshi, Tomohiro Aoyama, Kaoru Sato Extraction of topographic and material contrasts on surfaces from SEM images obtained by energy filtring detection with low-energy primary electrons Ultramicroscopy, 124 (2013) 20-25

[2] S. Mikmekova, B. Masek, H. Jirkova, D. Aisman, I. Mullerova, L. Frank. Microstructure of X210Cr12 steel after the forming in semi-solid state visualized by very low energy SEM in ultra high vacuum.Applied Surface Science, 275 (2013), 403-408

[3] D.A. Moncrieff, P.R. Barker, V.N.E.Robinson. Electron scattering by the gas in the scanning electron microscope J. Phys.D: Appl.Phys., 12 (1979), pp.481–488.

[4] F. Lenz. Scattering of medium energy electrons in very small angles. Zeitschrift Naturforschung, 9a (1954), pp.185–204

[5] G. Wentzel. Dispersion of corpuscular rays as diffraction appearances. Zeitschrift furPhysik, 40(1926), pp. 590–593

[6] R.E. Burge, G.H. Smith. A new calculation of electron scattering cross sections and a theoretical discussion of image contrast in the electron microscope. Proceeding of the physical society, 79(1962), pp. 673-690

[7] R. Gauvin. Some theoretical considerations on X-ray microanalysis in the environmental or variable pressure scanning electron microscope. Scanning, 21(1999), pp. 388-393

[8] R. Gauvin, D. Drouin. A formula to compute total elastic scattering Mott cross section. Sacnning, 15(1993), pp. 140-150.

[9] G.D. Danilatos. Environmental scanning electron microscopy and microanalysis. Mikrochimica Acta, 114-115 (1994), pp.143–155

[10] G.D. Danilatos. Foundations of environmental scanning electron microscopy. Advances in electronics and electron physics, 71, (1988). pp.109-250

[11] G.D. Danilatos. Equation of charge distribution in the environmental scanning electron microscopy ESEM Scanning Microscopy, 4(1990), pp. 799-823

[12] J. Rattenberger, J.Wagner, H.Schröttner, S. Mitsche, A. Zankel. A method to measure the total scattering cross section and effective beam gas path length in a low-vacuum SEM. Scanning, 31(2009), pp. 1–7.

[13] S.A. Wight, A.R. Konicek. Electron scattering cross section measurements in a variable pressure scanning electron microscope. Micron, 43(2012), pp.985–991.

[14] A. Kadoun, R. Belkorissat, B. Khelifa, C. Mathieu Comparative study of electron beam-gas interaction in an SEM operating at pressures up to 300 Pa. Vacuum, 69 (2003), pp. 537-543

[15] O. Mansour, K. Aidaoui, A. Kadoun, L. Khouchaf, C. Mathieu. Monte Carlo simulation of he electron beam scattering under gas mixtures environment in an HPSEM at low energy. Vacuum, 84 (2010), pp. 458-463

[16] K. Jost, J. Kessler. The spatial distribution of medium energy electrons during plural scattering. Zeitschrift Physik, 176(1963), pp. 126–142.

[17] F. Salvat, A. Jablonski, C.J. Powell. ELSEPA—Dirac partial-wave calculation of elastic scattering of electrons and positrons by atoms, positive ions and molecules. Computer Physics Communications, 165 (2005), pp.157–190

[18] F. Salvat. Optical-model potential for electron and positron elastic scattering by atoms. Phys. Rev. A., 68 (2003), pp. 012708

[19] E. Merzbacher. Quantum Mechanics, second ed John Wiley and Sons, New York, (1970)

[20] H. Feshbach. Theoretical Nuclear Physics: Nuclear Reactions. John Wiley and Sons, New York, (1992)

[21] J.F. Williams, B.A. Willis. The scattering of electrons from inert gases. I. Absolute differential elastic cross sections for argon atoms. J. Phys. B: At. Mol. Phys., 8(1975), pp. 1670

[22] S.K. Srivastava, H. Tanaka, A. Chutjian, and S. Trajmar Elastic scattering of intermediate-energy electrons by Ar and Kr. Phys. Rev. A., 23(1981), pp.2156

[23] D. DuBois and M. E. Rudd. Differential cross sections for elastic scattering of electrons from argon, neon, nitrogen and carbon monoxide. J. Phys. B: At. Mol. Phys., 9(1976), pp.2657

[24] J. Jansen, F. J. de Heer, H. J. Luyken, B. van Wingerden, H. J. Blaauw. Absolute differential cross sections for

elastic scattering of electrons by helium, neon, argon and molecular nitrogen. J. Phys. B: At. Mol. Phys., 9(1976), pp.185-212

[25] Panajotovic, D. Filipovic, B. Marinkovic, V. Pejcev, M. Kurepa, L. Vuskovic. Critical minima in elastic electron scattering by argon. J. Phys. B: At. Mol. Opt. Phys., 30(1997), pp.5877-5894.

[26] W.Wagenaar, A.de Boer, T.van Tubergen, J.Los, F.J.De Heer. Absolute differential cross sections for elastic scattering of electrons over small angles from noble-gas atoms. J. Phys. B: At.Mol.Phys., 19(1986), pp.3121.

[27] I. Iga, L.Mu-Tao, J.C.Nogueira, R.S.Barbieri Elastic differential cross section measurements for electron scattering from Ar and O2 in the intermediate-energy range J. Phys. B: At. Mol. Phys., 20(1987), pp. 1095

[28] S.C. Gupta, J.A. Rees. Absolute differential cross sections for 100 eV electrons elastically scattered by helium, neon, and argon. J. Phys. B: At. Mol. Phys., 8(1975), pp.1267

[29] W. McConkey, J.A. Preston. Differential elastic scattering of electrons by the rare gases. I. Helium J. Phys. B: At. Mol. Phys., 8(1975), pp.63

[30] D.F. Register, S. Trajmar, S. K. Srivastava. Absolute elastic differential electron scattering cross sections for He: A proposed calibration standard from 5 to 200 eV. Phys. Rev. A., 21(1980), pp.1134

[31] M.V. Kurepa, L. Vuskovic. Differential Cross Sections of 100, 150 and 200 eV Electron Elastically Scattered in Helium J. Phys. B: At. Mol. Phys., 8(1975), pp.2067

[32] G. Garcia, F. Arqueros, J. Camfos. Total cross sections for electron scattering from Ne, Ar and Kr in the energy range 70-6000 eV. J. Phys.B., 19 (1986), pp.3777.

[33] R.W. Wagenaar, F.J. de Heer. Total Cross Sections for Electron Scattering from Ar, Kr and Xe. J. Phys. B: At. Mol. Phys., 18(1985), pp. 2021-2036,

[34] W.E. Kauppila, T.S. Stein, J.H. Smart, M.S. Dababneh, Y.K. Ho, J. P. Downing, V. Po. Measurements of total scattering cross sections for intermediate-energy positrons and electrons colliding with helium, neon, and argon. Phys.Rev.A., (1981)24, pp.725.

[35] A. Zecca, P.G. Karwasz, R.S. Brusa. One century of experiments on electron-atom and molecule scattering: a critical review of integral cross-sections. Rivista del nuovo cimento, 19, N. 3(1996), pp.1-146

[36] H. Nishimura, K. Yano. Total Electron Scattering Cross Sections for Ar, $N_2$, $H_2O$ and $D_2O$. J. Phys. Soc. Japan, 57(1988), pp.1951.

[37] F.J. de Heer, R.H. Jansen. Total cross sections for electron scattering by He. J. Phys.B., 10(1977), pp.3741

[38] L. Boesten, H. Tanaka. Rational function fits to the nonresonant elastic differential cross sections (DCS) for e + He collisions, 0°–180°, 0.1 to 1000 eV. At.Data Nucl. Data Tables, 52 (1992), pp. 25-42

[39] M. Hayashi. Recommended values of transport cross sections for elastic collision and total collision cross section for electrons in atomic and molecular gases. Report IPPAM-19, Institute of Plasma Physics, Nagoya University, 1981.

[40] G. Dalba, P. Fornasini, I. Lazzizzera, G. Ranieri, A. Zecca Absolute total cross section measurements for intermediate energy electron scattering. I. He. J. Phys. B., 12 (1979), pp. 3787- 3795.

[41] G. Dalba, P. Fornasini, R. Grisenti, I. Lazzizzera., G. Ranieri, A. Zecca. Ramasuer type apparatus for absolute total cross section measurements at intermediate energy Rev. Sci. Instrum., 52 (1981) 979-983.

[42] J. He, D.C. Joy. Measurement of totals gas scattering cross section. Scanning, 25(2003), pp. 285-290